CFRP strengthening of butt-welded ultra-high strength steels under quasi-static tensile loading

Amraei Mohsen, Jiao Hui, Toghyani Amir, Björk Timo, Zhao Xiao-Ling

DOI: 10.1016/j.engstruct.2021.113052

Engineering Structures xxx (xxxx) 113052

Contents lists available at ScienceDirect

Engineering Structures

journal homepage: www.elsevier.com/locate/engstruct

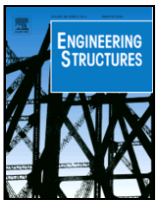

CFRP strengthening of butt-welded ultra-high strength steels under quasi-static tensile loading

Mohsen Amraei [a, b], Hui Jiao [c], Amir Toghyani [d], Timo Björk [b], Xiao-Ling Zhao [e, *]

[a] Reserach Group of Laser Material Processing and Additive Manufacturing, School of Energy Systems, LUT University, P.O. Box 20, 53851 Lappeenranta, Finland
[b] Laboratory of Steel Structures, Lappeenranta-Lahti University of Technology, P.O. Box 20, 53851 Lappeenranta, Finland
[c] School of Engineering and ICT, University of Tasmania, Hobart, TAS 7001, Australia
[d] Production Engineering Laboratory, Lappeenranta-Lahti University of Technology, P.O. Box 20, 53850, Lappeenranta, Finland
[e] The School of Civil and Environmental Engineering, UNSW Sydney, NSW 2052, Australia

ARTICLE INFO

Keywords:
Ultra-high strength steel (UHSS)
CFRP strengthening
Heat-affected zone (HAZ)
Mechanical properties

ABSTRACT

Due to the softening at the heat-affected zone (HAZ) in ultra-high strength steels (UHSS), the mechanical properties can deteriorate depending on the steels' grade, welding heat input, and its associated cooling rate. Hence, a design based on the properties of the base material (BM) may not be appropriate, and there is a need to retain the lost properties of the weldment. This study presents an effort to strengthen butt-welded UHSSs using ultra-high modulus (UHM) carbon fiber reinforced polymer (CFRP) plates. Although the rehabilitation and strengthening of steel structures using CFRPs have been available during the last two decades, they have not been used to strengthen higher grades of steel such as UHSSs. For this aim, a series of tensile tests were carried out on butt-welded UHSSs strengthened with adhesively bonded UHM CFRP plates on both sides of the weldment. Two welding processes, i.e. the gas metal arc welding (GMAW) and laser welding, were implemented separately to join the plates. Microhardness measurements and tensile tests were carried out for the experimental part, as well as finite element (FE) analysis of the joints. The results were also compared with other available methods, i.e. high-frequency mechanical impact (HFMI) treatment and TIG-dressing (tungsten inert gas) of the weld toe that are commonly used to increase the fatigue life of UHSS joints. It was found that CFRP strengthening can not only retain the lost properties of the weldment but can also increase the joint strength up to 32% compared to the BM, and a considerable 50% higher stiffness. In contrast, the other methods (HFMI and TIG-dressing) had no impact on the tensile characteristics of the weldments.

Nomenclature

A_0	Initial cross-section
A_{loss}	Void area
BM	Base material
CFRP	Carbon fiber reinforced polymer
D	Damage parameter
DIC	Digital image correlation
DSS	Double-side strengthened
EPPF	Effective plastic strain
EPPFR	Effective plastic strain at which the element deletes
F	Focal point position
FE	Finite element
f_u	Tensile strength
GMAW	Gas metal arc welding
HAZ	Heat-affected zone
HFMI	High-frequency mechanical impact
HI	Heat input
HSS	High strength steel
Hv	Vickers hardness
LW	Laser welding
I	Welding current
P	Tensile load
RD	Steel's rolling direction
TIG	Tungsten inert gas
t_{a1}	Adhesive thickness (first layer)
t_{a2}	Adhesive thickness (second layer)

* Corresponding author.
E-mail address: xiaolin.zhao@unsw.edu.au (X.-L. Zhao).

https://doi.org/10.1016/j.engstruct.2021.113052
Received 12 August 2020; Received in revised form 3 August 2021; Accepted 16 August 2021

t_s	Thickness of the steel substrate
t_{t1}	Thickness of the composite system after bonding the first layer
t_{t2}	Thickness of the composite system after bonding the second layer
UHM	Ultra-high modulus
UHSS	Ultra-high strength steels
V	Welding moving head speed
ε	Thermal efficiency of the welding procedure
ε_1, ε_2, ε_3	Principal plastic strains
$\sigma_{0.2\%}$	0.2% proof stress
$\sigma_{nominal}$	Nominal stress

1. Introduction

The applications of ultra-high strength steels (UHSS) (i.e. nominal yield strength over 690 MPa) are significantly increasing in structural engineering [1,2]. They have the desirable combination of high strength and low weight. However, their sensitivity to heat input (HI) from welding due to softening at the heat-affected zone (HAZ) can result in a decrease of static capacity, which reduces their efficiency [3].

Among the welding methods used in the literature to join UHSS plates and tubes, gas metal arc welding (GMAW) [4,5] and laser welding (LW) [6,7] were the most desirable. The tensile strength reduction of the joint due to the softened HAZ could go as high as 60% [8], which was dependent on the steel's grade and its manufacturing process [4], the executed welding method [6], HI, and cooling rate [3]. Nonetheless, the softened HAZ was negligible in all cases. Hence, it is vital to find possible solutions that can potentially retain the desirable characteristics of UHSS after welding.

The conventional method to rehabilitate or increase the fatigue life of metallic structures often involves bulky and heavy plates [9]. The other method that has gained attention in recent years, recommended by the International Institute of Welding (IIW), is the application of high-frequency mechanical impact (HFMI) treatment of the weld toe [10]. According to Yildirim and Marquis (2012), one fatigue class increase in strength (about 12.5%) for every 200 MPa increase in static yield strength for HFMI-treated welded joints is expected [11]. Although this method provides fatigue life extension for welded details, it is limited to fatigue crack initiation only [11]. Moreover, it has a depth effectiveness up to 1.5 mm, and it does not offer any increase in the static capacity of the welded joints [12]. Accordingly, it is important to find other solutions that can efficiently increase the load carrying capacity under static loading and enhance the fatigue life (both crack initiation and propagation phases) in such steel materials.

An alternative method, which recently became attractive as a strengthening solution for metallic structures, is the application of carbon fiber reinforced polymers (CFRPs) [13–15]. CFRPs were used to rehabilitate metallic members such as flexural strengthening of beams in bridge structures [16], cracked steel plates [17], welded plates [18], and welded hollow sections [19], with special attention paid to retrofitting aged bridge structures [20]. The steel grades strengthened by CFRP in the literature are limited to mild steel, with few examples of high strength steel (HSS) up to a grade of S690 [5,21], as well as a paper by Jiao and Zhao (2004) on the strengthening of UHSS circular hollow sections using CFRP sheets [22]. The investigation of CFRP strengthening welded UHSS is necessary partially because of the softening in the heat-affected zone (HAZ), which reduces the strength of the steel, and partially because such structures may need strengthening after some years of service due to degradation caused by corrosion or to increased service loading. The main concern in using CFRPs to strengthen higher grades of steel is premature debonding. Since UHSS undergoes much higher service loading, higher shear stress in the bond interface is expected. However, a study by Amraei et al. (2020) on UHSS thin plates suggests that the bond interface can carry loads up to the tensile strength of the base steel substrate when the plate thickness was below 10 mm [23]. Hence, it motivates further studies on the feasibility of CFRPs in strengthening UHSSs.

This research aims to strengthen butt-welded UHSS using CFRP plates. The steel plates were grades S700 and S960 manufactured via quenched and tempered and direct quenching, respectively. The direct quenched types of UHSS are especially prone to the negative effects of the welding HI [3]. Two welding methods, i.e. GMAW and LW, were adopted to join the plates of each steel grade together. The CFRP plates were made of unidirectional fibers with elastic modulus of 450 GPa. Araldite adhesive, which was found to be suitable for bonding UHSS and UHM CFRP, was utilized to manufacture the steel-CFRP composite specimens [24,25]. Furthermore, the results were compared with that of CFPR-strengthened mild steels and of HFMI and TIG-dressing treatment of the weldments. Moreover, the possible fatigue life extension of butt-welded UHSS strengthened with CFRP was examined. Finally, to evaluate the state of stress at the weld toe in strengthened specimens, the finite element analysis was performed using the LS-DYNA software package.

2. Materials

The weldments of two UHSSs (i.e. S700 and S960) were chosen to be strengthened using UHM CFRP under quasi-static loading. The nominal chemical compositions of the as-received steel plates are shown in Table 1 based on the certificates provided by the manufacturer.

Both steel alloys had a mixture of bainite (B) and martensite (M) in their microstructure, as shown in Fig. 1. More details of the microstructure of BMs can be found in [3,26]. Due to their low carbon content, these steel grades are suitable for welding. However, because of their fine microstructure, UHSS grades are more sensitive to the welding HI compared to the lower grades of steel [5]. Hence, the welding HI should be kept under 1 kJ/mm in each weld pass as recommended in the literature [3].

The UHM CFRP laminate chosen to strengthen the steel substrates had a nominal thickness and width of 2.27 and 50 mm, respectively. According to the manufacturer, Young's modulus and tensile strength of the CFRP laminate were 450 GPa and 1500 MPa, respectively. It is notable that the very high elastic modulus of such CFRP laminate is achievable only at strain values over 0.2%, as pointed out by Ghafoori and Motavalli [27]. In their study of a similar CFRP laminate from the same manufacturer, Young's modulus of the CFRP was calculated as 399 GPa, which was 11% lower than that claimed by the manufacturer.

In order to bond the CFRP laminate to the steel substrate, the two-part adhesive Araldite 420 A/B was used. Due to its superior properties, this adhesive is commonly used in bonding applications for metallic

Table 1
The nominal chemical composition of the BMs (wt. %).

Steel	C	Si	Mn	P	S	V	Cu	Cr	Ni	Mo	CEV*
S700	0.12	0.25	2.10	0.020	0.10	0.20	–	–	–	–	0.38
S960	0.088	0.04	1.13	0.010	0.000	0.009	0.011	1.00	0.05	0.117	0.59

*Carbon equivalent content

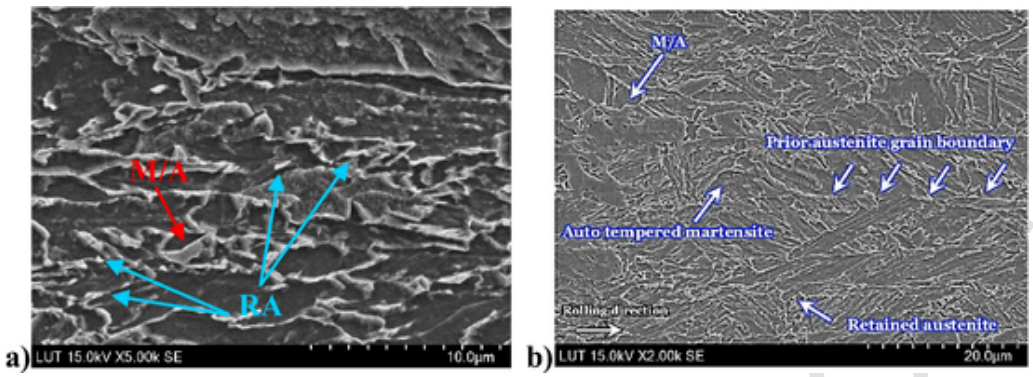

Fig. 1. SEM images of the BMs **a)** S700 [3], and **b)** S960 [26].

substrates. According to Fawzia [28], the shear strength and tensile modulus of the adhesive are 28.6 and 1901 MPa, respectively.

3. Experimental program

The experimental program in this study included four steps. First, a butt-welded joint was manufactured in which two welding methods, including GMAW and LW, were adopted. Next, tensile specimens were cut from the welded plates. After that, the composite system was fabricated, and the specimens were allowed to cure. Finally, the specimens were tensile tested at ambient conditions. The step-by-step procedure is explained in this section.

3.1. Welding

Two processes were implemented in this phase, including GMAW and LW. To attain consistent high-quality welding, the processes were performed using a robot arm. For the GMAW, a double V-groove profile was made by machining the plate's edge, as shown in Fig. 2. A welding torch passed at each side of the joint with a moving head speed of 6.2 mm/s. The welding filler material was chosen according to the tensile strength of steel so that a match configuration was reached for each steel grade. The welding torch was tilted to a 5° angle toward the pushing direction. Based on the welding parameters, the induced heat input energy of 0.7 kJ/mm for each weld pass was attained; it was calculated through [29], as shown in Eq. (1).

$$Q = \varepsilon \times U \times I/(v \times 1000)\ (kJ/mm) \quad (1)$$

According to Eq. (1), ε is the thermal efficiency of the welding procedure, which is 0.8 for GMAW. U, I, and v are the welding arc voltage, current, and moving head speed. The applied welding parameters are shown in Table 2.Table 3.

To laser weld the specimens, a 10-kW power fiber laser machine was utilized. The plate edges at the welded area were machined for 2 mm to remove possible HAZ due to the laser cutting process. Hence, a flat edge was manufactured, and the air gap was set to zero. A round shape with 0.2 mm radius was achieved as the laser beam was focused using a 300-mm lens and a collimation of 150 mm. The focal point position (F) was set at 3 mm below the surface, creating a keyhole shape at the cross-section of the weldment. Since no filler material was used in the LW process, the joint strength was at perfect match configuration compared to that of the BM. The laser beam was passing on the surface of the weldment with a speed of 30 mm/s, which is considered as a very fast welding process [3]. The applied welding parameters are listed in Table 2.

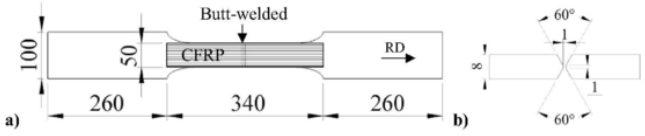

Fig. 2. Schematic of tensile specimens. a) Butt-welded with adhesively bonded CFRP (RD stands for steel's rolling direction), b) the double-V groove shape for GMAW. (Dimension in mm, not to scale).

Table 2
The applied welding parameters for GMAW and LW processes.

GMAW						
	Weld pass [No.]	**Filler material**	**I [A]**	**U [V]**	**V [mm/s]**	**Q [kJ/mm]**
S700	1	**Union Ni 2.5**	219	25.1	6.2	0.71
	2		219	25.1	6.2	0.71
S960	1	**Union X96**	214	25.1	6.2	0.69
	2		217	25.1	6.2	0.70
LW						
	Power **[kW]**	F **[mm]**	v **[mm/s]**		Q **[kJ/mm]**	
S700	9	−3	30		0.3	
S960						

Table 3
Measured thicknesses of all specimens (all in mm).

Specimen	t_s	t_c	$t_{t\,1}$	$t_{t\,2}$	t_{a1}	t_{a2}
S700 GMAW-DSS	8.01	2.27	10.73	13.43	0.45	0.43
S960 GMAW-DSS	8.23	2.27	10.95	13.63	0.45	0.41
S700 LW-DSS	8.01	2.27	10.68	13.39	0.40	0.44
S960 LW-DSS	8.22	2.27	10.97	13.68	0.48	0.44

3.2. Specimens

According to the experimental program in this study, five different specimens were manufactured, including

(a) BMs with no welds as control specimens
(b) GMAW and LW specimens with no CFRP strengthening scheme
(c) Welded specimens strengthened with CFRP on both sides
(d) GMAW specimens with no CFRP strengthening, treated at the weld toe using HFMI or TIG-dressing
(e) Butt-welded specimens (using GMAW) and strengthened on both sides using CFRP laminates.

For the BM specimens (a), the steel plates were laser cut in a rolling direction (RD) to form a flat dog-bone shape, as shown in Fig. 2 **(a)**. To manufacture welded specimens (b), two steel plates were butt-welded using either GMAW or LW. After the steel plates were welded, tensile specimens were laser cut, as shown in Fig. 2. In order to attain weld consistency in all welded specimens, the cut samples were taken from a single weldment manufactured by a robot arm. The effect of HI from

laser cutting at the edge in the reduced cross-section area was avoided by performing 2 mm of machining. The specimens for CFRP strengthening (c) were cut from the same weldment as those in (b) so that the weld quality is kept consistent. The details of the composite system manufacturing are explained in section 3.3. HFMI and TIG-dressing were performed at the weld toe of the GMAW specimen in the S960 specimen only (d). Since no strength reduction is reported after welding the S700 steel in the literature [3], these treatments were only applied to the S960 steel substrate. Both treatments were performed manually using the forehand technique with a tilt angle of 60–90°. Details of such treatments can be found in the literature [30].

3.3. Composite system fabrication

The steel plates were strengthened on both sides, and the whole length between the grips was covered by CFRP, as shown in Fig. 2. Since CFRP laminates were adopted for this purpose, the surface of the steel substrate at the weld area needed to be smoothed out. Accordingly, the weld reinforcements on both sides were machined. The grinding process was performed to smooth the surface of the specimen. According to the literature [23,25], the bond length between UHM CFRP and steel is about 100–120 mm. To avoid premature debonding, a bond length of 170 mm was adopted in this paper.

After smoothing the weld region, the surface of the steel at the bonding region was sandblasted. This helped to enhance the surface roughness and to achieve an adequate interlocking between the CFRP and the steel. The sandblasted region was then cleaned using an acetone solvent, and the adhesive layer was applied to the surface of the steel. Next, the CFRP surface was cleaned using acetone prior to attaching it to the steel surface. Finally, the CFRP was placed in its position, and a uniform pressure was applied to the entire surface to squeeze out any air bubbles. The composite system was kept clamped for a week in an ambient condition. The preparation of the second layer followed the same procedure. The thickness of the adhesive layer was controlled at 0.4 mm using spacing by cut metal wires according to the recommendations in the literature [23].

The thickness of the composite system was measured after bonding each layer to determine the adhesive thickness, as shown in Table 4. The terms t_{a1}, t_{t1}, t_s, and t_c stand for the thickness of the first adhesive layer, the composite system after bonding the first layer, steel, and CFRP, respectively. The thickness of the second layer was measured accordingly by replacing t_{t1} with t_{t2} and t_{a1} with t_{a2}, which stand for total thickness after bonding both layers and thickness of the second adhesive layer, respectively. The specimens were labeled as BM, GMAW, LW and GMAW-DSS, and LW-DSS, which stand for the base material only, GMAW and LW with no CFRP, and double-side strengthened configurations after GMAW and LW, respectively. The letter "S" and the number in front of it represent the steel's grade.

Table 4
Details of the specimens in this study.

Steel grade	Welding method	Treatment method	Testing method	Number of specimens
S700	None	none	Quasi-static	1
	GMAW	none	Quasi-static	1
		CFRP strengthened	Quasi-static	1
	LW	none	Quasi-static	1
		CFRP strengthened	Quasi-static	1
S960	Non	none	Quasi-static	1
	GMAW	none	Quasi-static	1
		none	Fatigue	2
		HFMI	Quasi-static	1
		TIG	Quasi-static	1
		CFRP strengthened	Quasi-static	1
		CFRP strengthened	Fatigue	2
	LW	none	Quasi-static	1
		CFRP strengthened	Quasi-static	1
Total number of specimens				16

3.4. Testing

3.4.1. Tensile testing

The tensile properties of the specimens were determined using quasi-static tension tests. For this aim, a 1200 kN tensile testing machine with displacement control was used. The strain rate of the test was kept constant at $4 \times 10^{-5}\ s^{-1}$. A digital image correlation (DIC) system was utilized to measure the strain distribution on the surface of the specimens during tensile testing. The DIC system worked with two optical cameras directed toward the surface of the specimen, on which a stochastic pattern of black dots was sprayed on a white painted base. During the test, a software (GOM) measured the distance between the black dots and transferred that onto a strain contour. To measure the strain values both on the surface and at the through-thickness of the specimens, the cameras were tilted in an inclined 25° angle toward the specimen. Details of the DIC system and its calibration are explained in [23]. The test was continued until the failure of the steel substrate.

3.4.2. Fatigue testing

To study the possible fatigue life extension of the welded UHSS, two specimens were CFRP-strengthened under uniaxial constant amplitude cyclic loading. The stress ration of the loading was 0.1, with an applied stress range of 594 MPa. The specimen preparation followed the same procedure as explained in **section 3.3**. The results were then compared with the available data in the literature on butt-welded and cut-edge specimens made of UHSS (i.e. S960 and S1100). Table 4 shows the details of both quasi-static and fatigue tests of this paper.

3.4.3. Microhardness measurement

The Vickers hardness values at the through-thickness of welded specimens were measured to examine the softening/hardening effect of the welding at the HAZ. For this aim, the cross-section of welded specimens was ground and polished. At first, grinding was performed using abrasive particles with a roughness of 120 μm for four minutes. Next, another four minutes of grinding was performed using diamond particles with a roughness of 9 μm. A final polishing was performed for six minutes using fine diamond particles with a roughness of 3 μm. Finally, the specimen was etched with Nital 5% for 15 s. After polishing, Vickers micro-indentation hardness was performed using a Durascan 70 machine. A load of 5 kgf and a dwell period of 10 s was applied. The hardness points were collected along three horizontal lines at the through-thickness, including 1 mm below the surface, at the mid-section, and 1 mm above the bottom of the cross-section, simply named top, middle, and bottom, respectively. For the GMAW specimens, the top and bottom lines represented the second and first weld passes, respectively.

4. Numerical simulation

Finite element (FE) modeling using the LS-DYNA software package in explicit time integration was implemented [31]. Four steps were included in the FE analysis, including

- simulation of the base steel substrates
- welded specimens with consideration of various material properties for the HAZ
- bond modeling between UHM CFRP and UHSS
- welded UHSS strengthened with UHM CFRP.

In all sections, an eight-node hexahedral solid element with constant stress formulation was used. The mesh size in the descritization of the model was chosen so that the element size matched that of the DIC measurement. The mechanical properties of the BMs were driven from uniaxial tensile tests. In the FE modeling, an elasto-visco-plastic material model with isotropic hardening behavior [31] was assigned to the steel substrates. In this model, damage was considered before the rupture point, and the failure was defined based on a pre-defined strain [31]. When the failure strain in tension was reached, directional damage started and evolved in either one or two orthogonal directions until rupture. Once the rupture strain was detected at all integration points, the element was removed.

The damage parameter (D) was related to the plastic strain at which the softening of the elements starts and ends with the following equation:

$$D = \frac{\varepsilon^p - EPPF}{EPPFR - EPPF} \tag{2}$$

where $\varepsilon^p$is the state of plastic strain, EPPF is the effective plastic strain at which material softening begins, and EPPFR is the effective plastic strain at which the element deletes. "D" is a scalar value ranging between zero (no damage has happened) and one (fully damaged). The strain at rupture is calculated based on the von Mises formula:

$$\varepsilon = \sqrt{2/3(\varepsilon_1{}^2 + \varepsilon_2{}^2 + \varepsilon_3{}^2)} \tag{3}$$

in whichε_1, ε_2, and ε_3 represent the principal plastic strains of the element.

The nominal stress in the damaged material was calculated according to Eq. (4), given by

$$= \frac{P}{A_0} \tag{4}$$

in which P is tensile load, and A_0 is the initial cross-section. The true stress at the damaged material was calculated considering the void area (A_{loss}) by

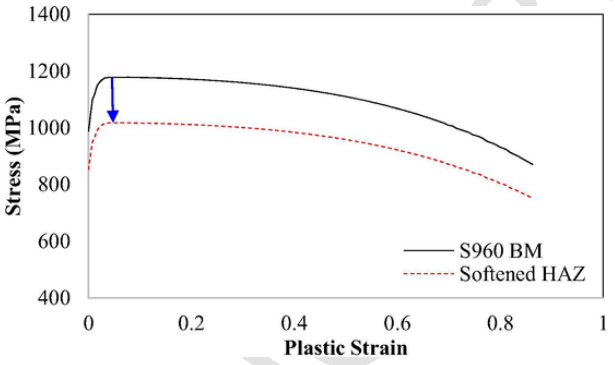

Fig. 3. The stress-plastic strain curve of the BM and softened HAZ in S960.

$$= \frac{P}{A_0 - A_{loss}} \tag{5}$$

To define material properties of the softened HAZ, the tensile strength was first calculated based on the relationship between strength and hardness. According to Murakami [32],

$$0.5f_u = 1.6Hv \pm 0.1Hv \tag{6}$$

in which f_u is tensile strength in MPa, and Hv is the Vickers hardness. Finally, the BM stress–strain curve was shifted down by the fraction of the ultimate strength at the HAZ compared to that of the BM, as shown in Fig. 3. According to the literature, the down shifting of the tensile characteristics of S960 at the softened HAZ is proven to happen [26].

To define the geometry of each area such as the BM, HAZ, and fusion zone, the microhardness measurements as images of the polished cross-section were used. The final geometry of each zone was meshed, as shown in Fig. 4.

The bond model between UHSS and UHM CFRP was implemented according to the proposal by Amraei et al. (2019) [23]. In that model, the EPPFR was considered to be five times as EPPF, which was also proposed by Wu et al. (2012) [25]. In the current analysis, with respect to the mesh size used in the paper, EPPFR was 0.25, as proposed by Fawzia et al. (2010) [28], and shear strength and tensile modulus of the adhesive were considered as 28.6 and 1901 MPa, respectively. No damage was considered for the CFRP plates, as the failure mode in all specimens was debonding at the adhesive layer. In order to bond the surfaces together (CFRP to adhesive, and adhesive to steel substrate), the mesh size was chosen in such a way that nodes coincided together. Hence, by merging the nodes, the surfaces were tied together.

5. Results and discussion

5.1. Microhardness evaluation

The hardness measurement profiles of the weldments are shown in Fig. 5. In the GMAW process, since the upper face was welded first, the second weld pass (at the bottom) has widened the HAZ at the top [3]. Hence, the hardness profile in Fig. 5 focuses on the measurement along this line. For the LW, both the top and bottom profiles show almost identical values.

The S700-GMAW steel shows a relatively low reduction (13%) in the magnitude of its hardness at the weld HAZ. Using the welding parameters in this study, the softened HAZ has a total length of 2.5 mm after two weld passes. Due to its high cooling rate, the S700-LW specimen shows a minor softening at the HAZ and a major hardening at the fusion zone.

On the other hand, the S960 steel alloy shows a great reduction in its hardness after being welded, regardless of the type of joining process. The maximum hardness reduction at the softened HAZ of GMAW and LW specimens are 32% and 23%, respectively. However, it is noticeable from the hardness profiles that the width of the HAZ is considerably different in these two welding methods. While the two weld passes of

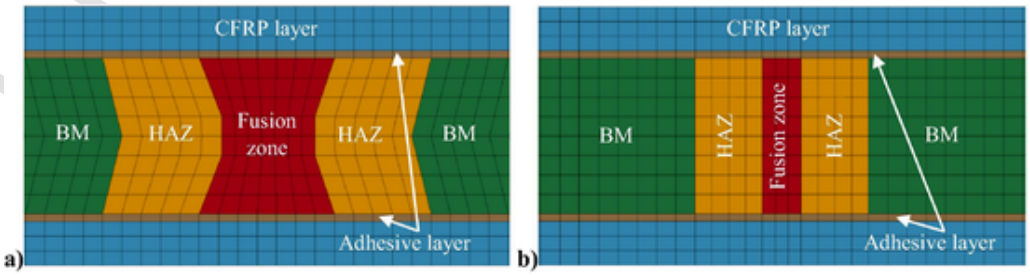

Fig. 4. Discretization of elements at the through-thickness in FE models of CFRP strengthened welded specimens, **a)** GMAW and **b)** LW.

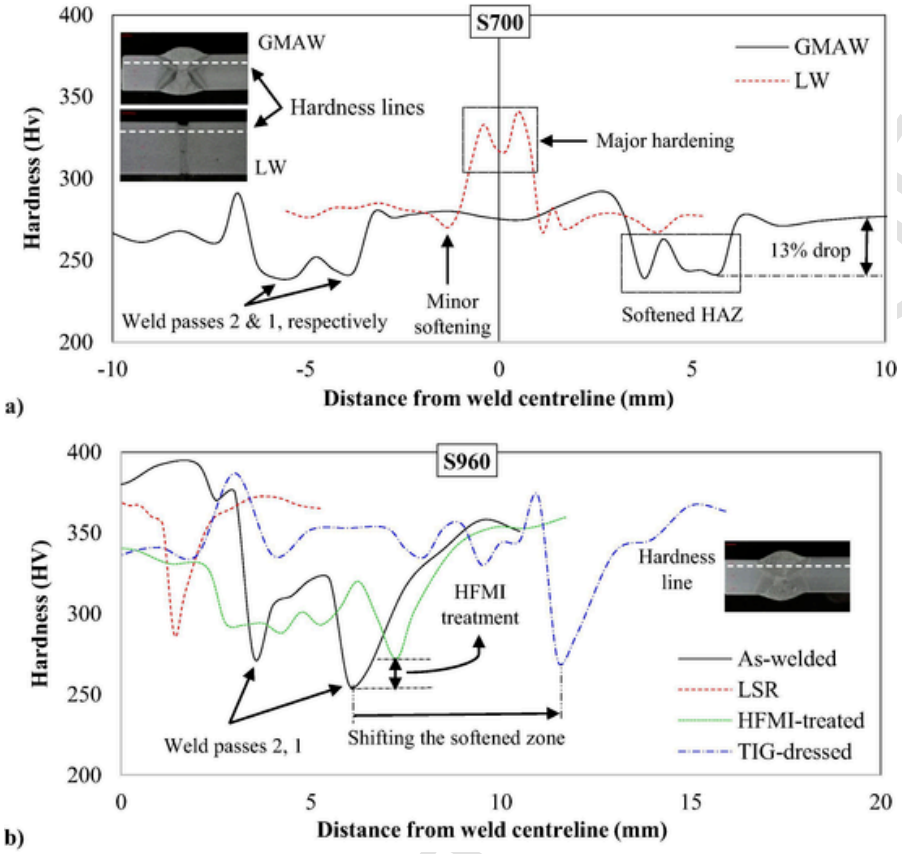

Fig. 5. Hardness distribution across the weldments at 1 mm below upper surface, **a)** S700 and **b)** S960.

GMAW have created a wide HAZ with a 7 mm length, the LW specimen has a narrow HAZ with total length of 1.8 mm. The post-welding treatments, i.e. HFMI and TIG-dressing, have a minor impact on the magnitude of hardness. Both treatments show a maximum 10% increase in the hardness value at the softened HAZ compared to the as-welded condition. However, a 6 mm shift in the location of the HAZ is noticeable from Fig. 5**b**.

5.2. Tensile test results

The tensile test results of the specimens are shown in Fig. 6. Regardless of the joining process, the S700 steel alloy shows no strength reduction after being welded. However, the displacement at the rupture point decreases depending on the welding process. While the GMAW specimen fails after 20 mm of displacement, the LW specimen has almost reached the rupture strain of the BM. The changes in ductility and strain at the rupture point has also been pointed out by Amraei et al. (2019) [3]. The reason is that the weld reinforcement in GMAW acts as a boundary condition, limiting the flow of plastic strains throughout the entire gauge area [26]. Due to the smooth surface in the LW specimen (as no weld reinforcement exists), the plastic strain flows freely on the specimen, leading to higher ductility.

On the other hand, the ultimate tensile strength of CFRP-strengthened S700 weldment is 32% higher than the BM, as seen in Fig. 6**(a)**. Simultaneously, the strengthened joint has a 53% higher Young's modulus (305 GPa). A two-stage failure mechanism occurred during tensile testing of the CFRP-strengthened specimens. At first, the excessive shear stress at the bond interface caused end-debonding of the CFRP laminates, as shown in Fig. 7**(e)**. This resulted in a severe drop in the magnitude of loading, as can also be seen in Fig. 6. Next, the specimen acted like a non-strengthened joint following the same load–displacement path. However, since the CFRP laminates were still

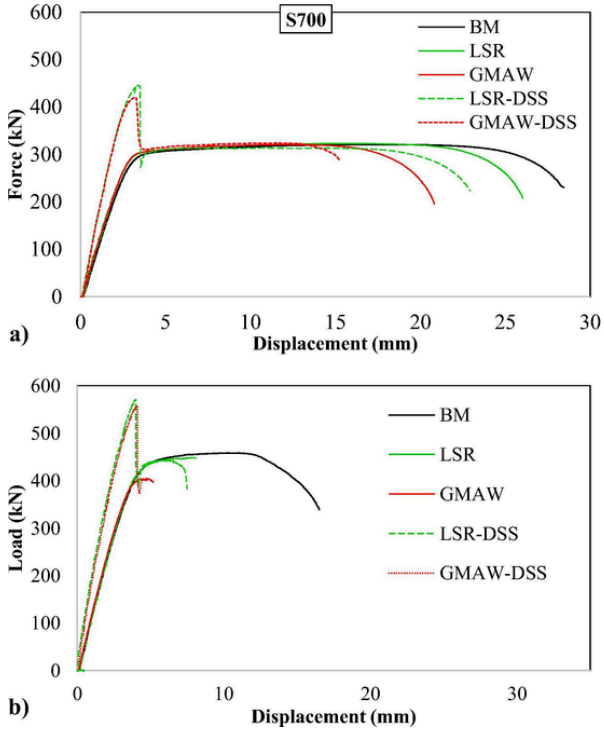

Fig. 6. Tensile test results of the specimens, **a)** S700 and **b)** S960.

in touch with some areas, the stress flow was partially limited throughout the specimen; thus, failure occurred in a lower displacement.

According to the classification in the literature, the failure mode in the CFRP-strengthened metallic structures can be categorized as (a)

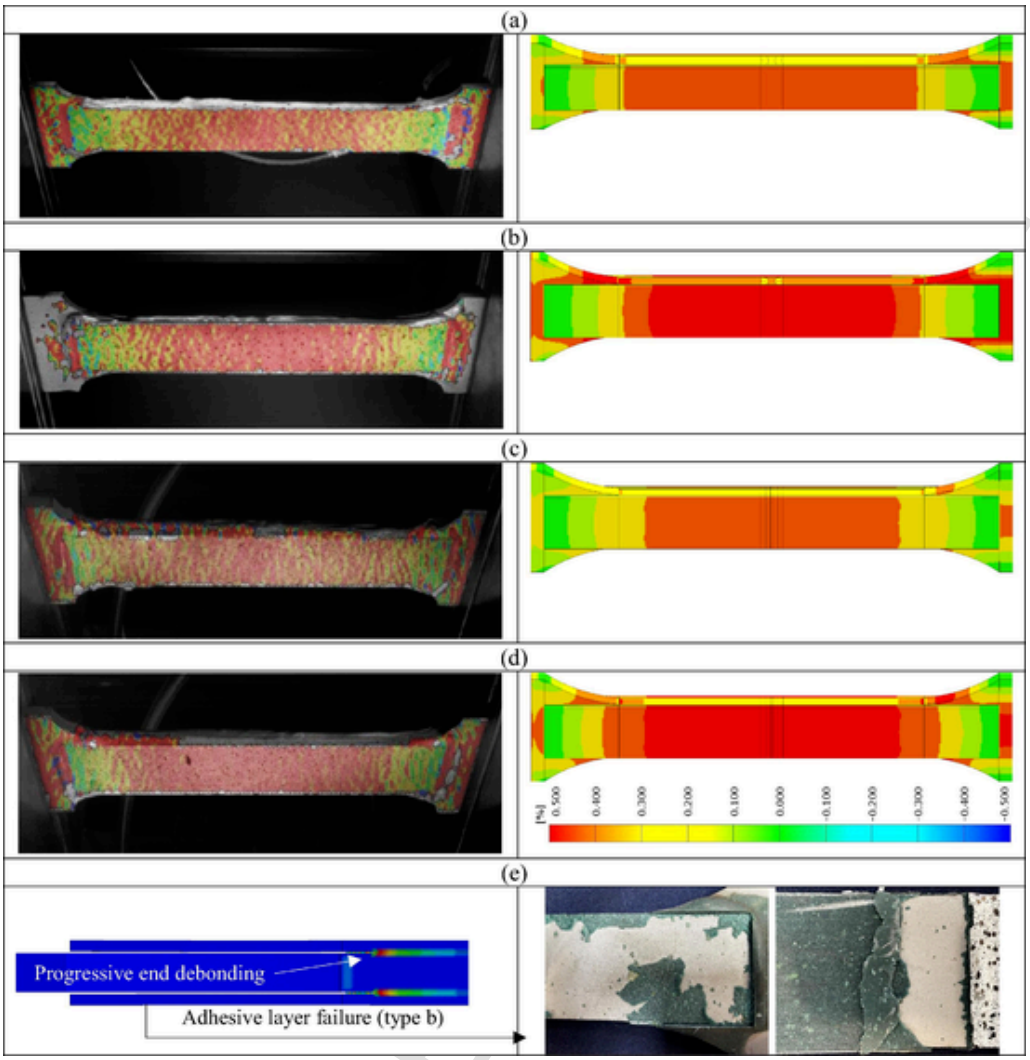

Fig. 7. Distributions of the strains at the debonding point for CFRP strengthened specimens. **a)** S700-GMAW, **b)** S960-GMAW, **c)** S700-LW, and **d)** S960-LW (From left to right, DIC and FE, respectively, and **e)** end debonding and examples of adhesive layer failure (type b).

steel and adhesive interface failure; (b) cohesive failure (adhesive layer failure); (c) CFRP and adhesive interface failure; (d) CFRP delamination; (e) CFRP rupture; and (f) steel yielding [33]. The failure mode of all specimens in the current study was type (b), adhesive layer failure as shown in Fig. 7 **(e)**. It is notable that there are various configurations in which CFRP bonded to steel substrate can be tested under quasi-static loading conditions [33–36]. The current study method is that loading is directly applied to the steel element without any gap. A schematic drawing of such loading a condition is shown in Fig. 8.

In contrast, the as-welded S960 specimens revealed reduction in both proof stress ($\sigma_{0.2\%}$) and ultimate tensile strength (f_u) due to the softened HAZ. The degree of reduction in tensile strength varied depending on the applied welding process (and its associated cooling rate) and joint type (butt or fillet weld) [37]. While the GMAW specimen showed a 13–14% reduction in both proof stress and tensile strength, the tensile strength reduction in LW was almost 5%. However, a great reduction in the ductility of S960 weldments is visible, especially for the GMAW process, in which the joint has almost lost its elongation capacity. Although the LW specimen showed higher ductility compared to the GMAW specimen, it still suffered from the lack of elongation capacity [3].

The CFRP-strengthened S960 specimens showed 23% and 55% higher tensile strength and modulus of elasticity, respectively, compared to the BM. This is especially considerable since the welded speci-

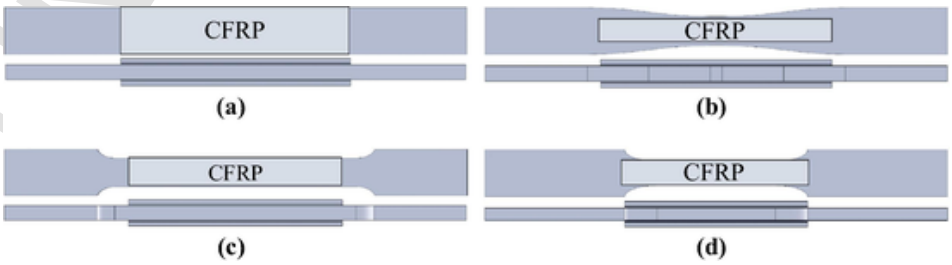

Fig. 8. Schematic view of different testing conditions that loading is directly applied to the steel element without any gap, **(a)** uniform width [34], **(b)** dog-bone shape [35], **(c)** coupon shape [36], and **(d)** this paper.

mens lost part of their strength after being welded. Hence, if the composite joint strength is compared with the as-welded condition, the tensile strength for GMAW and LW specimens has increased to 42% and 28%, respectively. However, no major change in displacement at the rupture point of the specimens was observed. The two-stage failure mechanism also occurred in the strengthened S960 specimens, as seen in Fig. 6**(b) and 7**. Similarly, the cohesive failure at the adhesive layer was also observed in CFRP-strengthened S960 specimens.

5.3. Comparison with results in the literature

A comparison of the results on the strengthened joints (both S700 and S960) with the available data in the literature shows that the degree of strengthening depends on the steel's grade. Al-Emrani et al. (2005) conducted a series of tests on the strengthening of BMs made of mild steel, which were strengthened with various CFRP and adhesive types [35], like the configuration in Fig. 8**(b)**. In their study, a 76–80% increase in the tensile capacity of the mild steel-composite system is reported [35], which is higher compared to the UHSS composite in this study.

On the other hand, according to Colombi and Poggi [36], much lower bond strength was achieved when mild steel plates were strengthened on both sides using normal-modulus CFRP plates in a configuration like Fig. 8**(c)**. According to their results, the maximum bond strength per unit width of the composite system was 1.97 kN/mm [36]. This value is much lower than the results of this study, which shows 4.24 and 5.57 kN/mm of bond strength per unit width for S700 and S960 specimens, respectively.

The results were also compared with the thin UHSS tubes (1.60 mm), strengthened with five layers of CFRP sheets (thickness and Young's modulus of 0.13 mm and 230 GPa, respectively) [22]. Although the full capacity of the butt-welded joint was recovered, no increase in the joint's strength compared with the BM was reported. On the other hand, the butt-welded UHSS plates in this study showed considerable strength enhancement compared to the BM when UHM CFRP plates were utilized.

Besides the degree of strengthening, the failure mechanism in mild steel composite systems [35,36] was different compared to strengthened high-strength steel plates [21] and the current research on UHSS. While the rupture of CFRP laminates (type e) was observed when UHM CFRP plates were used to strengthen mild steel [35], cohesive failure (type b) was observed in the current study. The two-stage failure (like this study) was reported in the case of a normal-modulus CFRP laminate-mild steel configuration [35]. However, according to Colombi and Poggi [36], yielding the steel substrate followed by the interfacial debonding of the steel-adhesive layer (type a) governed the failure of the normal-modulus CFRP-mild steel composite system.

Like UHSS, when the S690 high-strength steel plates specimen similar to the configuration (a) in Fig. 8 were strengthened with three layers of UHM CFRP sheets, a type (b) failure was reported [21]. Due to its superior strength, no yielding occurred up to the debonding point of both S700 and S960 steel substrates in this study.

5.4. HFMI and TIG-dressing

The tensile test results of the HFMI-treated and TIG-dressed specimens are shown in Fig. 9, which provides insight into the comparison with the CFRP-strengthening method. As can be seen, no major changes in the tensile characteristics of the post-weld treated specimens has occurred. In HFMI specimens, the treatment effect is only limited on the surfaces, yet the through-thickness hardness remains almost intact [12]. Hence, under high-tensile loading, the treatment effect does not compensate the through-thickness–softened HAZ, and the specimen behaves similarly to the as-welded condition. However, if the loading is in the range of fatigue design, then HFMI treatment can offer a considerable life enhancement as mentioned in the literature [11].

Similarly, the TIG-dressed specimen does not offer any change to the tensile characteristics of the specimen. The only major change is shift-

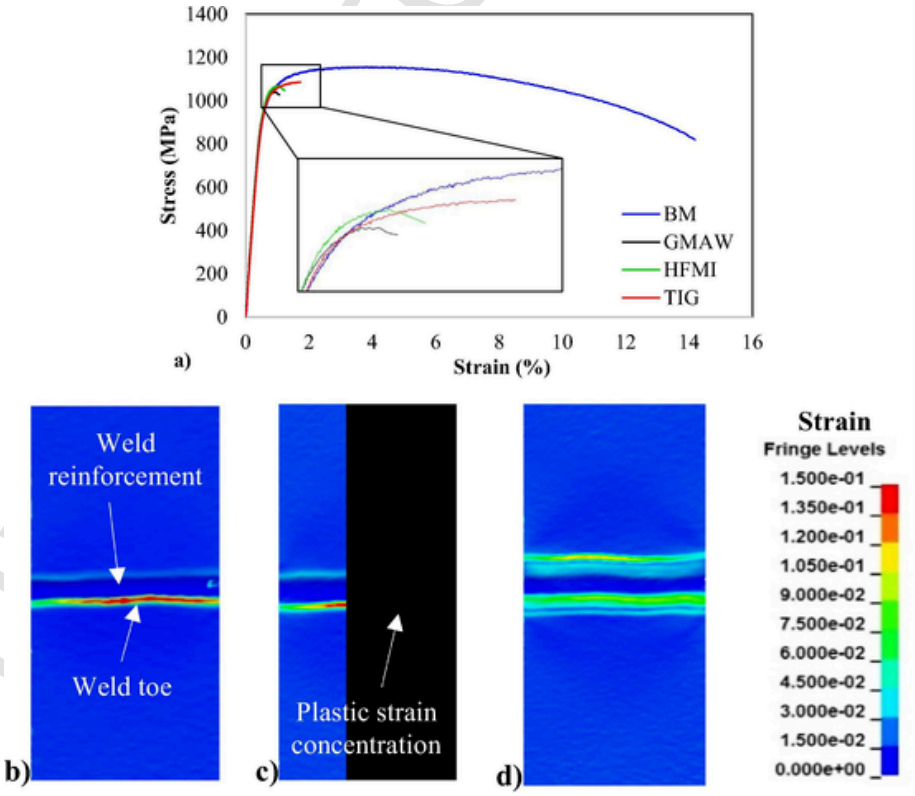

Fig. 9. Tensile test results of the post welding treatments on S960 steel alloy, **a)** engineering stress–strain curves, and the distribution of strain on the surface by Aramis: **b)** as-welded GMAW, **c)** HFMI treated, and **d)** TIG-dressed.

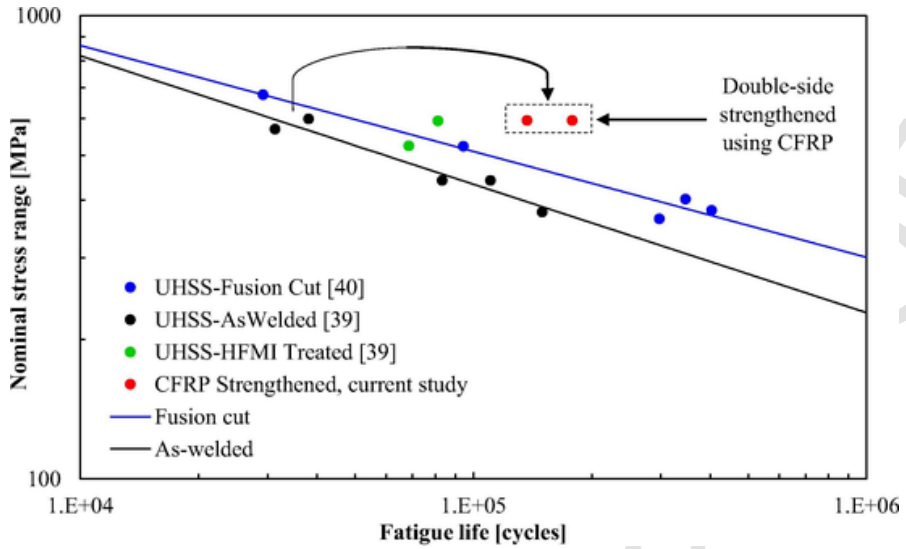

Fig. 10. Fatigue life evaluation of welded UHSS.

ing the location of the softened HAZ, as shown in the hardness profile graph (Fig. 5**(b)**) and the geometrical change of the weld toe radius. Although the geometrical change would influence the fatigue characteristics of the weld, it does not offer any improvement in the static capacity of the joint. As seen from Fig. 9 **(b**, **c**, and **d)**, the plastic stress concentrated at the softened HAZ on the weld toe led to the premature failure of the joint.

5.5. Possible fatigue life enhancement

Under fatigue loading, the mechanisms by which HFMI treatment and TIG-dressing work is different compared to CFRP strengthening. While compressive residual stress on the surface and geometrical changes at the weld toe, respectively, govern the fatigue life in HFMI treatment and TIG-dressing, the CFRP strengthening directly reduces the tensile loading from the through-thickness of the joint.

According to the FE analysis of composite joints, when the load reaches the tensile strength of the BM, the tensile stress at the HAZ of S700 and S960 specimens was 437 and 587 MPa, respectively. These values are far below the ultimate strength of the GMAW specimens (725 and 922 MPa), which is more than a 60% reduction. Hence, a great fatigue enhancement is envisioned for such joints due to the reduction of the stress at the weld HAZ by the CFRP plates. If the slope of the fatigue curve (m) is considered to be 3 (according to the IIW recommendations) [38], the fatigue life of such joints is expected to reach at least 5 times that. Similarly, the work on butt-welded high-strength square hollow sections strengthened with normal-modulus CFRP plates shows that the fatigue life of strengthened joints were 4–5 times higher than unstrengthened ones depending on the applied stress range [5].

This is also evident from the experimental results of the fatigue tests shown in Fig. 10. There are four categories of specimens, including butt-welded specimens in as-welded condition [39], cut-edge specimens (using fusion cut) with no welding [40], HFMI-treated specimens [39], and butt-welded UHSS double-side strengthened with CFRP (current study). As shown, the fatigue life of CFRP-strengthened specimens is extended to values even over the life of cut-edge specimens. For HFMI-treated specimens, the fatigue life has reached the life of a fusion-cut specimen. However, since the treatment is only at the weld toe, the microcracks at the cut edge cause the fatigue failure of specimens. However, in CFRP strengthening, since nominal stress is reduced at the whole cross-section, a higher fatigue life has been reached.

6. Conclusion

This paper deals with the strengthening of butt-welded UHSS using adhesively bonded UHM CFRP plates under quasi-static tensile loading. For this aim, specimens were manufactured using two welding methods, i.e. GMAW and LW, that cause different degrees of softening at the HAZ. The specimens were then strengthened on both sides of the weldment in which the entire gauge between the grips was covered by a layer of UHM CFRP plates. To investigate the efficiency of CFRP strengthening compared with other available methods, HFMI-treated and TIG-dressed weldments were also tensile tested. According to the results, the following conclusions were drawn:

- The degree of softening was different at the studied steel alloys and the associated welding methods. The welded S700 showed a relatively low hardness reduction (maximum 13%) at the HAZ, while it was up to 32% for S960.
- Regardless of the joining process, the S700 steel alloy showed no strength reduction under tensile loading after being welded.
- Welded S960 specimens revealed reduction in both $\sigma_{0.2\%}$ and f_u. The strength reduction for GMAW and LW was 14% and 5%, respectively.
- The greatest impact of welding was on the ductility of the welded S960 as rupture occurred at elongation under 5%.
- The ultimate tensile loading capacity of the welds after strengthening increased for 28–42%, depending on the steel grade and welding method.
- The stiffness of the joints increased for 53–55% after CFRP strengthening.
- A two-stage failure mechanism occurred during tensile testing of the CFRP-strengthened specimens. At first, the excessive shear stress at the bond interface caused end-debonding of the CFRP laminates, in which the adhesive layer failed cohesively. Next, the specimen acted like a non-strengthened joint up to the final rupture.
- Both treatment methods, i.e., HFMI and TIG-dressing of the weld toe, showed no impact on the tensile characteristics of the weldment.

According to the FE analysis, the tensile stress at the HAZ of CFRP-strengthened specimens at an ultimate tensile loading equivalent to the BM remained in the elastic region. Hence, a considerable fatigue life enhancement is envisioned for the CFRP-strengthened specimens depending on the bond performance at high cycles. The limited experimental

fatigue tests conducted in this paper also demonstrated the possibility of an increasing fatigue life for values even over the base material. Accordingly, the authors suggest further investigation on the fatigue life of CFRP-strengthened UHSS weldments in various weld details and configurations.

CRediT authorship contribution statement

Mohsen Amraei: Conceptualization, Data curation, Formal analysis, Investigation, Methodology, Software, Validation, Writing – original draft, Writing – review & editing. **Hui Jiao:** Conceptualization, Methodology, Writing – review & editing. **Amir Toghyani:** Data curation, Investigation, Methodology, Validation, Writing – review & editing. **Timo Björk:** Conceptualization, Funding acquisition, Investigation, Methodology, Project administration, Resources, Supervision, Validation, Writing – review & editing. **Xiao-Ling Zhao:** Conceptualization, Funding acquisition, Investigation, Methodology, Project administration, Resources, Supervision, Validation, Writing – review & editing.

Declaration of Competing Interest

The authors declare that they have no known competing financial interests or personal relationships that could have appeared to influence the work reported in this paper.

Acknowledgment

The authors would like to appreciate financial support of Business Finland through ISA-LUT project, and the Australian Research Council through a Discovery Project (DP150100442). The authors wish to thank SSAB Europe Co. by providing the steel plates for this research. Special thanks to the technical support of the staff members at Laboratory of Steel Structures, Laboratory of Welding Technology of LUT University. The help and support of Matti Koskimäki, Antti Ahola and Olli-Pekka Pynnönen is highly appreciated.

References

[1] Ban H, Shi G. A review of research on high-strength steel structures. Proc. Inst. Civ. Eng. - Struct. Build. 2018;171:625–41. https://doi.org/10.1680/jstbu.16.00197.
[2] Liu X, Chung KF, Ho HC, Xiao M, Hou ZX, Nethercot DA. Mechanical behavior of high strength S690-QT steel welded sections with various heat input energy. Eng. Struct. 2018;175:245–56. https://doi.org/10.1016/j.engstruct.2018.08.026.
[3] Amraei M, Ahola A, Afkhami S, Björk T, Heidarpour A, Zhao XL. Effects of heat input on the mechanical properties of butt-welded high and ultra-high strength steels. Eng. Struct. 2019;198:109460. https://doi.org/10.1016/j.engstruct.2019.109460.
[4] Guo W, Li L, Dong S, Crowther D, Thompson A. Comparison of microstructure and mechanical properties of ultra-narrow gap laser and gas-metal-arc welded S960 high strength steel. Opt. Lasers Eng. 2017;91:1–15. https://doi.org/10.1016/j.optlaseng.2016.11.011.
[5] Amraei M, Jiao H, Zhao XL, Tong LW. Fatigue testing of butt-welded high strength square hollow sections strengthened with CFRP. Thin-Walled Struct. 2017;120:260–8. https://doi.org/10.1016/j.tws.2017.09.004.
[6] Farrokhi F, Siltanen J, Salminen A. Fiber Laser Welding of Direct-Quenched Ultrahigh Strength Steels: Evaluation of Hardness, Tensile Strength, and Toughness Properties at Subzero Temperatures. J. Manuf. Sci. Eng. Trans. ASME. 2015;137. https://doi.org/10.1115/1.4030177.
[7] Guo W, Crowther D, Francis JA, Thompson A, Liu Z, Li L. Microstructure and mechanical properties of laser welded S960 high strength steel. Mater. Des. 2015;85:534–48. https://doi.org/10.1016/j.matdes.2015.07.037.
[8] Jiao H, Zhao XL, Lau A. Hardness and compressive capacity of longitudinally welded very high strength steel tubes. J. Constr. Steel Res. 2015;114:405–16. https://doi.org/10.1016/j.jcsr.2015.09.008.
[9] Tavakkolizadeh M, Saadatmanesh H. Fatigue Strength of Steel Girders Strengthened with Carbon Fiber Reinforced Polymer Patch. J. Struct. Eng. 2003;129:186–96. https://doi.org/10.1061/(ASCE)0733-9445(2003)129:2(186).
[10] Marquis GB, Mikkola E, Yildirim HC, Barsoum Z. Fatigue strength improvement of steel structures by high-frequency mechanical impact: Proposed fatigue assessment guidelines. Weld. World. 2013;57:803–22. https://doi.org/10.1007/s40194-013-0075-x.
[11] Yildirim HC, Marquis GB. Fatigue strength improvement factors for high strength steel welded joints treated by high frequency mechanical impact. Int. J. Fatigue. 2012;44:168–76. https://doi.org/10.1016/j.ijfatigue.2012.05.002.
[12] Mikkola E, Marquis G, Lehto P, Remes H, Hänninen H. Material characterization of high-frequency mechanical impact (HFMI)-treated high-strength steel. Mater. Des. 2016;89:205–14. https://doi.org/10.1016/j.matdes.2015.10.001.
[13] W.G. Cadei, J.M.C.; Stratford, T.J.; Hollaway, L.C.; Duckett, Strengthening Metallic Structures Using Externally Bonded Fibre-reinforced Composites: Cadei, J. M. C., Stratford, T. J., Hollaway, L.C., Duckett, W. H.: 9780860175957: Amazon.com: Books, CIRIA. (2004). https://www.amazon.com/Strengthening-Structures-Externally-Fibre-Reinforced-Composites/dp/0860175952 (accessed September 2, 2020).
[14] Zhao X-L. FRP-Strengthened Metallic Structures - 1st Edition - Xiao-Ling Zhao -. Gr: Taylor Fr; 2013. https://www.routledge.com/FRP-Strengthened-Metallic-Structures/Zhao/p/book/9781138074330 (accessed September 2, 2020).
[15] Teng JG, Yu T, Fernando D. Strengthening of steel structures with fiber-reinforced polymer composites. J. Constr. Steel Res. 2012;78:131–43. https://doi.org/10.1016/j.jcsr.2012.06.011.
[16] Siwowski TW, Siwowska P. Experimental study on CFRP-strengthened steel beams. Compos. Part B Eng. 2018;149:12–21. https://doi.org/10.1016/j.compositesb.2018.04.060.
[17] Aljabar NJ, Zhao XL, Al-Mahaidi R, Ghafoori E, Motavalli M, Powers N. Effect of crack orientation on fatigue behavior of CFRP-strengthened steel plates. Compos. Struct. 2016;152:295–305. https://doi.org/10.1016/j.compstruct.2016.05.033.
[18] Liu H, Zhao XL. Prediction of fatigue life for CFRP strengthened steel connections under combined loads. Int. J. Struct. Stab. Dyn. 2013;13. https://doi.org/10.1142/S0219455412500599.
[19] Fam A, Witt S, Rizkalla S. Repair of damaged aluminum truss joints of highway overhead sign structures using FRP. Constr. Build. Mater. 2006;20:948–56. https://doi.org/10.1016/j.conbuildmat.2005.06.014.
[20] Ghafoori E, Motavalli M, Nussbaumer A, Herwig A, Prinz GS, Fontana M. Design criterion for fatigue strengthening of riveted beams in a 120-year-old railway metallic bridge using pre-stressed CFRP plates. Compos. Part B Eng. 2015;68:1–13. https://doi.org/10.1016/j.compositesb.2014.08.026.
[21] Hu LL, Zhao XL, Feng P. Fatigue Behavior of Cracked High-Strength Steel Plates Strengthened by CFRP Sheets. J. Compos. Constr. 2016;20:4016043. https://doi.org/10.1061/(ASCE)CC.1943-5614.0000698.
[22] Jiao H, Zhao XL. CFRP strengthened butt-welded very high strength (VHS) circular steel tubes. Thin-Walled Struct. 2004;42:963–78. https://doi.org/10.1016/j.tws.2004.03.003.
[23] Amraei M, Zhao XL, Björk T, Heidarpour A. Bond characteristics between high/ultra-high strength steel and ultra-high modulus CFRP laminates. Eng. Struct. 2020;205:110094. https://doi.org/10.1016/j.engstruct.2019.110094.
[24] Fawzia S, Al-Mahaidi R, Zhao XL. Experimental and finite element analysis of a double strap joint between steel plates and normal modulus CFRP. Compos. Struct. 2006;75:156–62. https://doi.org/10.1016/j.compstruct.2006.04.038.
[25] Wu C, Zhao X, Duan WH, Al-Mahaidi R. Bond characteristics between ultra high modulus CFRP laminates and steel. Thin-Walled Struct. 2012;51:147–57. https://doi.org/10.1016/j.tws.2011.10.010.
[26] Amraei M, Afkhami S, Javaheri V, Larkiola J, Skriko T, Björk T, et al. Mechanical properties and microstructural evaluation of the heat-affected zone in ultra-high strength steels. Thin-Walled Struct. 2020;157:107072. https://doi.org/10.1016/j.tws.2020.107072.
[27] Ghafoori E, Motavalli M. Normal, high and ultra-high modulus carbon fiber-reinforced polymer laminates for bonded and un-bonded strengthening of steel beams. Mater. Des. 2015;67:232–43. https://doi.org/10.1016/j.matdes.2014.11.031.
[28] Fawzia S, Zhao XL, Al-Mahaidi R. Bond-slip models for double strap joints strengthened by CFRP. Compos. Struct. 2010;92:2137–45. https://doi.org/10.1016/j.compstruct.2009.09.042.
[29] EN 1011-1, EN 1011-1 - Welding - Recommendations for welding of metallic materials - Part 1: General guidance for arc welding, (2009). https://standards.globalspec.com/std/1165734/EN 1011-1 (accessed September 3, 2020).
[30] T. Skriko, Dependence of manufacturing parameters on the performance quality of welded joints made of direct quenched ultra-high-strength steel, PhD thesis, Department of Mechanical Engineering,Lappeenranta University of Technology, 2018. https://lutpub.lut.fi/handle/10024/158538.
[31] LS-DYNA Keyword User's Manual, (2014).
[32] Y. Murakami, Metal Fatigue: Effects of Small Defects and Nonmetallic Inclusions - 2nd Edition, 1st ed., 2002. https://www.elsevier.com/books/metal-fatigue-effects-of-small-defects-and-nonmetallic-inclusions/murakami/978-0-12-813876-2.
[33] Zhao XL, Zhang L. State-of-the-art review on FRP strengthened steel structures. Eng. Struct. 2007;29:1808–23. https://doi.org/10.1016/j.engstruct.2006.10.006.
[34] Miller TC, Chajes MJ, Mertz DR, Hastings JN. Strengthening of a Steel Bridge Girder Using CFRP Plates. J. Bridg. Eng. 2001;6:514–22. https://doi.org/10.1061/(ASCE)1084-0702(2001)6:6(514).
[35] M. Al-Emrani, D. Linghoff, R. Kliger, Bonding strength and fracture mechanisms in composite steel-CFRP elements, in: Proc. Int. Symp. Bond Behav. FRP Struct., Hong Kong, China, 2005.
[36] Colombi P, Poggi C. Strengthening of tensile steel members and bolted joints using adhesively bonded CFRP plates, in. Constr. Build. Mater., Elsevier 2006;22–33. https://doi.org/10.1016/j.conbuildmat.2005.06.042.
[37] T. Peltoniemi, The effect of stress concentration on the ultimate capacity of welded joints made of ultra-high strength steel, LUT Univ. (2016). https://lutpub.lut.fi/handle/10024/130064 (accessed September 2, 2020).
[38] A.F. Hobbacher, Recommendations for fatigue design of welded joints and components, in: IIW Docu, 2016: p. 148. https://doi.org/10.1007/978-3-319-23757-2_1.

[39] Pirinen H. Fatigue strength of welded joints made of S1100 structural steel. Lappeenranta University of Technology; 2019.
[40] Lipiäinen K, Ahola A, Skriko T, Björk T. Fatigue strength characterization of high and ultra-high-strength steel cut edges. Struct: Accepted for publication by Eng; 2020.